WILEY

RESEARCH ARTICLE

Modulation of network-to-network connectivity via spike-timing-dependent noninvasive brain stimulation

Emiliano Santarnecchi[1,2] | Davide Momi[2] | Giulia Sprugnoli[2] | Francesco Neri[2] |
Alvaro Pascual-Leone[1] | Alessandro Rossi[2] | Simone Rossi[2,3]

[1]Berenson-Allen Center for Non-Invasive Brain Stimulation, Division of Cognitive Neurology, Department of Neurology, Harvard Medical School, Boston, Massachusetts

[2]Brain Investigation and Neuromodulation Laboratory, Unit of Neurology and Clinical Neurophysiology, Department of Medicine, Surgery and Neuroscience, Siena School of Medicine, Siena, Italy

[3]Human Physiology Section, Department of Medicine, Surgery and Neuroscience, University of Siena, Siena, Italy

Correspondence
Emiliano Santarnecchi, Berenson-Allen Center for Noninvasive Brain Stimulation, Harvard Medical School, Department of Cognitive Neurology, Beth Israel Deaconess Medical Center, 330 Brookline Avenue, KS-450, Boston, MA 02215.
Email: esantarn@bidmc.harvard.edu

Abstract

Human cognitive abilities and behavior are linked to functional coupling of many brain regions organized in distinct networks. Gaining insights on the role those networks' dynamics play in cognition and pathology requires their selective, reliable, and reversible manipulation. Here we document the possibility to manipulate the interplay between two brain networks in a controlled manner, by means of a Transcranial Magnetic Stimulation (TMS) protocol inducing spike timing dependent plasticity (STDP). Pairs of TMS pulses at specific inter-stimulus intervals, repeatedly delivered over two negatively correlated nodes of the default mode network (DMN) and the task-positive network (TPN) defined on the basis of individual functional magnetic resonance imaging (fMRI) data, induced a modulation of network-to-network connectivity, even reversing correlation from negative to slightly positive in 30% of cases. Results also suggest a baseline-dependent effect, with a greater connectivity modulation observed in participants with weaker between-networks connectivity strength right before TMS. Finally, modulation of task-evoked fMRI activity patterns during a sustained attention task was also observed after stimulation, with a faster or slower switch between rest and task blocks according to the timing of TMS pulses. The present findings promote paired associative TMS as a promising technique for controlled manipulation of fMRI connectivity dynamics in humans, as well as the causal investigation of brain-behavior relations.

KEYWORDS

brain connectivity, brain stimulation, default mode network, fMRI, plasticity, resting-state networks

1 | INTRODUCTION

The human brain constantly integrates internal and external stimuli by means of oscillatory dynamics occurring at different time and spatial scales (Raichle, 2015). Such complex pattern of inter-regional interactions have shown similarities with other biological complex networks, like its capacity for simultaneous local and distributed information processing (Eguiluz, Chialvo, Cecchi, Baliki, & Apkarian, 2005; Sepulcre et al., 2010) and the power-law distribution of network nodes

importance (Achard & Bullmore, 2007; Eguiluz et al., 2005; Gallos, Makse, & Sigman, 2012). Most importantly, spontaneous brain activity can be decomposed into separate but integrated resting-state networks (RSNs) (Achard & Bullmore, 2007; Sporns, 2011) also known as "modules" (Power et al., 2011) or "architectures" (Hearne, Cocchi, Zalesky, & Mattingley, 2017), with specific RSNs reflecting the activity within sensory (i.e., visual, motor, and auditory) and associative brain regions related to high-order cognitive processes, such as abstract reasoning, attention, language, and memory. This organization, as

captured via functional connectivity (FC) analysis of functional magnetic resonance imaging (fMRI) data collected during resting-state (rs-fMRI), is correlated with individual variability in several cognitive functions and personality traits (Adelstein et al., 2011), with recent studies suggesting the possibility of even capturing individual brain's uniqueness by means of finely tailored FC analysis (Finn et al., 2015). Most importantly, changes in such intrinsic connectivity emerge when pathological states arise (Altamura et al., 2012; Anderson et al., 2011), suggesting rs-fMRI as a useful tool to predict disease progression as well as to characterize connectivity patterns correlated with specific symptomatology (Boes et al., 2015; Fischer et al., 2016). All together, these evidences suggest the importance of mapping the human connectome and its pathology-specific alterations. Even more crucially, tools to selectively manipulate network dynamics must be developed and validated, possibly leading to future therapeutic approaches.

In the last three decades, noninvasive brain stimulation (NIBS) techniques have been successfully used to transiently modify brain activity (Hallett, 2007). For instance, transcranial magnetic stimulation (TMS) of a single cortical target has been shown to induce modifications of specific co-activation patterns (Eldaief, Halko, Buckner, & Pascual-Leone, 2011; Halko, Farzan, Eldaief, Schmahmann, & Pascual-Leone, 2014; Wang et al., 2014; Gratton, Lee, Nomura, & D'Esposito, 2013), while single pairs of TMS pulses over two connected brain regions have been used to causally probe inter-regional functional relationships (Arai et al., 2011; Pascual-Leone & Walsh, 2001; Koch, Ponzo, Di, Caltagirone, & Veniero, 2013). Additionally, associative stimulation based on repeated cortical and peripheral stimulation (e.g., TMS over the primary motor cortex coupled with electrical stimulation of the median nerve; paired associative stimulation, PAS; Stefan, Kunesch, Benecke, Cohen, & Classen, 2002) has been shown to induce prolonged modifications of cortico-spinal excitability. In a conceptually similar manner, but focused on cortico-cortical association, pairs of TMS pulses at appropriate inter-stimulus intervals (ISIs) (e.g., 200 paired TMS pulses over brain regions "A" and "B" with an ISI of 10 ms; cortico-cortical PAS [ccPAS]) can induce modulation of inter-regional coupling according to spike-timing dependent plasticity (STDP) mechanisms (in particular long-term potentiation, LTP; Abbott & Nelson, 2000; Buch, Johnen, Nelissen, O'Shea, & Rushworth, 2011), with some recent evidence also suggesting corresponding behavioral changes in the motor and visual systems (Romei, Chiappini, Hibbard, & Avenanti, 2016). The mechanism(s) of action for PAS follows the principles of Hebbian plasticity (Koch et al., 2013), assuming that a TMS pulse (pulse A) over a given region (e.g., the left dorsolateral prefrontal cortex [DLPFC]) will activate the targeted region, resulting in spiking activity reaching other functionally connected regions. Being the timing between the two TMS pulses (i.e., ISI) appropriate, when spikes from the left DLPFC reach the second TMS target (e.g., left inferior parietal lobule, IPL) a second TMS pulse (pulse B) is delivered over the parietal cortex, resulting in strengthening of DLPFC-IPL connection via LTP mechanism. When repeated over time, after effects due to reinforcement of synaptic efficacy between the two stimulated sites are observed, with a stronger modulation of A over B. Cortico-cortical PAS constitutes a suitable tool for brain connectivity modulation, but its potential application to study large-scale connectivity dynamics has not been explored yet. In

fact, the current literature is focused on the modulation of inter-regional dynamics within the sensorimotor (e.g., premotor to motor cortex, somatosensory to motor) and visual system, with the exception of a recent study investigating fronto-parietal dynamics using simultaneous TMS and electroencephalography (EEG) recording (TMS-EEG) (Casula, Pellicciari, Picazio, Caltagirone, & Koch, 2016). Moreover, the typical application of ccPAS protocols is based on the measurement of electrophysiological or behavioral changes involving the activity of the receiving end of the network being stimulated (i.e., increase in motor evoked potentials, MEPs, recorded on the motor cortex after conditioning ccPAS applied to premotor [A] and motor cortex [B]), hence providing no evidence of the feasibility of a direct modulation of A↔B dynamics in terms of changes in their functional connectivity. The possibility to transiently modulate fMRI-based connectivity between brain regions outside the motor and visual systems would open up the possibility of modulating altered connectivity patterns characterizing neurological and psychiatric conditions (Greicius, 2008), as well as potentially manipulate cognitive networks in the healthy brain (Sporns, 2014). However, this requires the direct investigation of network-to-network activity in response to ccPAS, assessing the specificity of A ↔ B modulation by also exploring the activity of the rest of the brain instead of focusing only on the regions being stimulated (as in the case of motor and visual paradigm using TMS-based output measures).

Here we tested whether prolonged ccPAS of two fMRI network nodes in the frontal and parietal lobes might lead to the selective modulation of their spontaneous coupling, as measured via FC fMRI analysis (Figure 1a). To this aim, we used a double-coil neuronavigated TMS system to target the default mode network (DMN) and the so-called task positive network (TPN), whose negative connectivity has been linked to both normal cognitive functioning (Spreng, Stevens, Chamberlain, Gilmore, & Schacter, 2010) and optimal healthy aging (Spreng, Stevens, Viviano, & Schacter, 2016). Moreover, the connectivity between the DMN and TPN has been recently linked to neurodegenerative disorders (Zhou et al., 2010). In particular, a study comparing patients with frontotemporal dementia (FTD) and Alzheimer's disease (AD) has shown a link between the severity of patients' cognitive decline and the magnitude of increased (in FTD) or decreased (in AD) DMN ↔ TPN negative connectivity, thus suggesting the external modulation of DMN–TPN interplay as a potential novel therapeutic option. Therefore, to test the feasibility of modulating network connectivity in humans, nodes of the DMN and the negatively correlated TPN were targeted by applying a previously validated ccPAS protocol (targets "t^{DMN}" and "t^{TPN}" hereafter, Figure 1a,b; Fox et al., 2005; Uddin, 2014). Resting-state fMRI FC data were collected before and right after stimulation. TMS targets were defined based on individual FC patterns. We hypothesized that a change in FC right after ccPAS will be observed, but only for STDP-inducing ISI (e.g., ISI = +10 ms) and not for a "not-associative" control condition (ISI = 0 ms, i.e. simultaneous stimulation over t^{DMN} and t^{TPN}; t^{DMN} = t^{TPN} hereafter). To control for the order of TMS stimulation during STDP-inducing ccPAS, pairs of pulses were delivered according to two possible directions of connectivity modulation: (i) ISI = +10 ms, targeting the DMN node in the parietal lobe first (t^{DMN} → t^{TPN} hereafter), and (ii) ISI = −10 ms, targeting the frontal
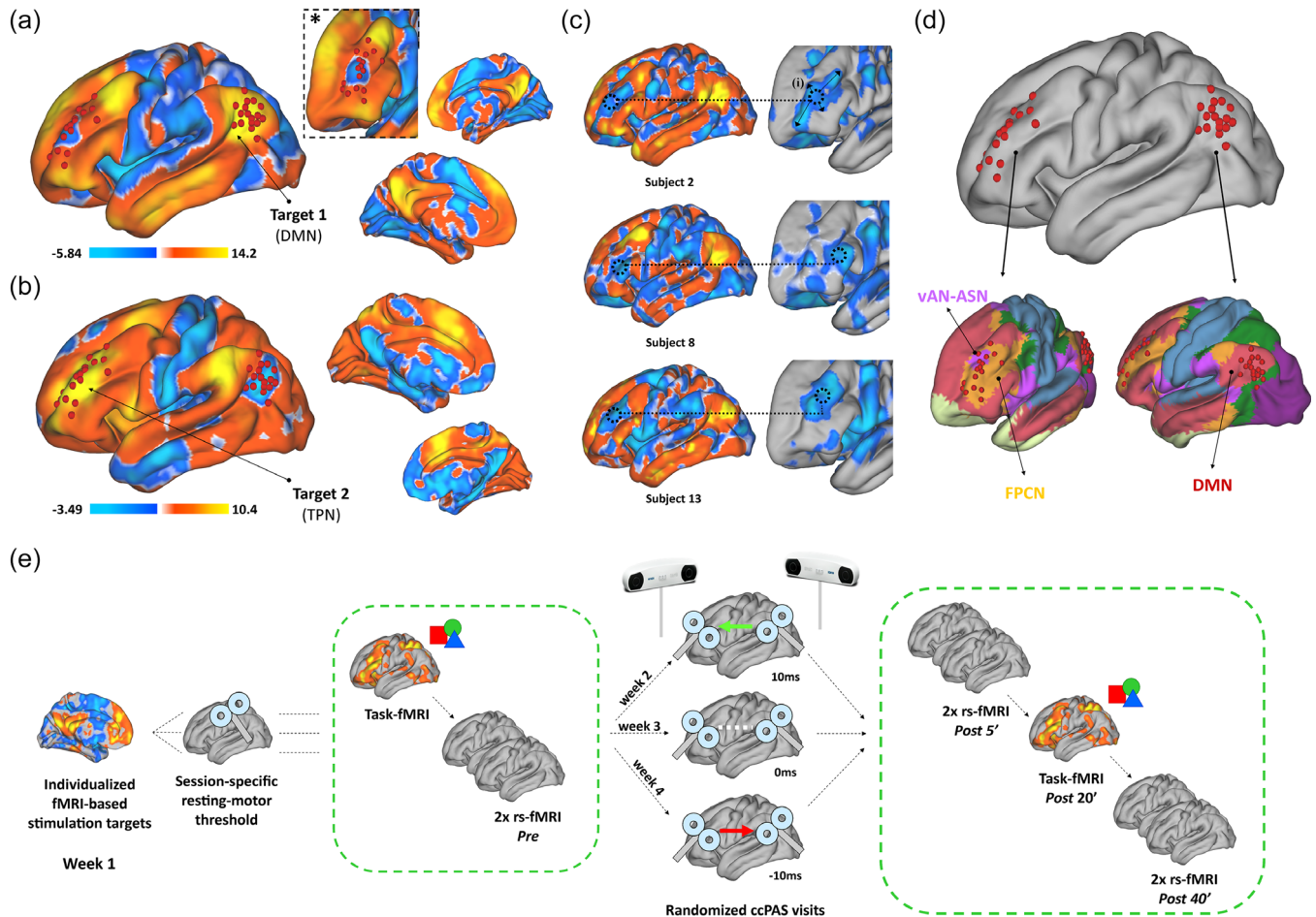
FIGURE 1 Stimulation sites and experimental design. (a,b) group-average functional connectivity profiles of stimulation sites in the DMN (t^{DMN}) and TPN (t^{TPN}) are shown, with red spheres representing individualized stimulation sites. As visible in *, the area negatively correlated with the DMN in the left frontal lobe at the group level does not match individual stimulation site, suggesting the value of individual target mapping as shown in (c). Stimulation sites t^{DMN} and t^{TPN} were manually identified according to individual rs-fMRI maps, minimizing source of error during TMS by selecting the centroid of the strongest negatively correlated spot for each participant (*i*). (d) t^{DMN} matches the topography of the DMN as described in Yeo et al. (2011), while t^{TPN} mostly overlap with the vAN and FPCN in Yeo et al. (2011) and the ASN as described in Shirer et al. (2012) (also see Supporting Information Figure S1). Panel (e) summarizes the experimental design, including individual targets selection, pre and post-interventions fMRI recording, the three stimulation sessions testing different ISI (+10 ms, 0 ms, and −10 ms) in random order across participants over a 3-weeks period (Week 2–3–4). Stimulation sites were based on baseline rs-fMRI data acquired on a separate experimental session (Week 1). TMS paired pulses intensity was adjusted at 90% and 120% of resting motor threshold, conventionally measured before each ccPAS session. Note: DMN, default mode network; TPN, task positive network; FPCN, frontoparietal control network; vAN, ventral attention network; ASN, anterior salience network; color bars report z-transformed FC values [Color figure can be viewed at wileyonlinelibrary.com]

lobe first ($t^{TPN} \rightarrow t^{DMN}$ hereafter). For details about the rationale for ISI selection, the procedure for individualized TMS targets' selection, and the different PAS protocols, see Section 2.

Finally, given the additional role attributed to the switch between DMN and TPN during attention-demanding tasks (for a review see Raichle, 2015), fMRI data were collected during a sustained attention task before and after each fMRI-ccPAS session (Figure 1e), as an additional exploratory aim of the study. Given the resemblance between individual spontaneous and task-evoked connectivity patterns (Tavor et al., 2016), a modulation of fMRI activations during the attention task was expected also after ccPAS. This might potentially lead to higher or lower "synchrony" between the two networks at rest, thus affecting the time required to switch between brain states while performing the cognitive task (i.e., from DMN-related "Rest" to TPN-related "Attention" blocks, and vice versa).

2 | MATERIAL AND METHODS

2.1 | Experimental design and Hebbian plasticity

The study was aimed at comparing the longitudinal effect of ccPAS applied over the two cortical regions (t^{TPN} and t^{DMN}) by using different inter-stimulus intervals (ISI). Specifically, a TPN node mostly loading on the anterior salience network (ASN; Dosenbach et al., 2007) was chosen for each participant (see Figure 1b and Supporting Information Figure S1). The coordinates of individual resting-state fMRI (rs-fMRI) maps identifying the most negatively correlated DMN and TPN nodes were implemented in two stereotaxic neuronavigation systems for positioning the TMS coils (see Figure 1c,d, Supporting Information Figure S1; see dedicated paragraph below and Supporting Information Materials).

The mechanism of PAS action implies the notion of Hebbian plasticity (Koch et al., 2013), assuming that a TMS pulse (pulse A) over, for example, t^{DMN} will activate the targeted region, resulting in spiking activity reaching other functionally connected regions. Being the timing between the two TMS pulses (i.e., ISI) appropriate, when t^{DMN} spikes reach the second TMS target, that is, t^{TPN}, a second TMS pulse (pulse B) is delivered over t^{TPN}, resulting in strengthening of t^{DMN}–t^{TPN} connection via LTP mechanism. Therefore, any ccPAS protocol requires exact notion about location and timing of the TMS pulses to be delivered. For the present investigation, the ISI was selected according to previous PAS experiments performed on very similar parieto-frontal sites (Casula, Pellicciari, Picazio, Caltagirone, & Koch, 2016). Moreover, LTP processes might reflect (i.e., be favored) by pre-existing spontaneous dynamics between regions A and B, with a stronger influence exerted by one of the two regions over the other. This might favor the occurrence of externally induced LTP via ccPAS. However, given the exploratory nature of the present investigation and the lack of knowledge about the hierarchy of t^{DMN}–t^{TPN} spontaneous co-modulation, the directionality of TMS pulses was defined in order to mimic the two possible "communication" directions, over two separate study visits: (i) posterior → anterior, with the first and second pulse being delivered respectively over the parietal and frontal lobes (i.e., parieto-frontal ccPAS, ISI = +10 ms, $t^{DMN} \rightarrow t^{TPN}$), mimicking a greater modulation exerted by the parietal over the frontal lobe; and (ii) anterior → posterior (i.e., fronto-parietal ccPAS, ISI = −10 ms, $t^{TPN} \rightarrow t^{DMN}$), assuming a greater modulation played by the frontal lobe. This is a common design in ccPAS experiments in humans where, in the absence of real-time electrophysiological data, both solutions are tested (Casula et al., 2016; Koch et al., 2013).

Finally, to account for potentially independent changes in FC due to local TMS effects over the two sites (e.g., a local effect of repetitive TMS over t^{DMN}, which could mask those induced by ccPAS), a "nonassociative" control condition based on simultaneous t^{DMN} and t^{TPN} stimulation was also tested and compared with those inducing STDP (i.e., ISI = 0 ms, $t^{DMN} = t^{TPN}$) (Figure 1e).

2.2 | Statistical analysis

A repeated measure Analysis of Variance (rp-ANCOVA) design was implemented for each of the different data types. Specifically, separate rp-ANCOVA models were built for functional connectivity fMRI data, effective connectivity fMRI data and task-fMRI data, testing the effect of factor "ISI" (3 levels = +10 ms, −10 ms, 0 ms) and "TIME", with the latter representing the different rs-fMRI runs acquired before and after ccPAS (3 levels = pre, post-5′, post-40′; Figure 1e). The analysis of task-fMRI data also included the impact of factor "BRAIN STATE" (2 levels = Attention, Rest), reflecting the two conditions tested during a sustained attention task performed in the scanner (Figure 1). Additional details about statistical model and analysis are reported in specific sections below.

2.3 | Participants

The study was approved by the Local Ethic Committee at the "Le Scotte" Hospital and University of Siena School of Medicine (Siena, Italy). Each participant provided written informed consent and was compensated 90€ for the entire study. Participants were 21 healthy individuals (11 males, 10 females; age M/SD = 24.2 ± 4 years) recruited through flyer and online posting, with normal vision and no history of neurological or psychiatric conditions. Each participant filled a TMS and MRI screening questionnaire before consenting for the study. Four participants did not complete all the TMS/MRI sessions due to drop-out or noisy functional connectivity maps making impossible to define reliable TMS targets. They were excluded from the analysis, thus resulting in a final sample of 17 participants.

2.4 | Stimulation sites identification

Modulation of rs-fMRI networks requires extreme precision because of individual differences in fMRI patterns (Fox, Halko, Eldaief, & Pascual-Leone, 2012). Only few studies have used intrinsic fMRI connectivity to identify TMS targets (for an example see Eldaief et al., 2011). Here we defined stimulation sites by collecting structural and functional MRI data on each participant (Week 1, Figure 1) and identifying the most negatively correlated nodes of the default mode network (DMN) and task positive network (TPN), by visually inspecting individual seed-based functional connectivity (FC) maps (Fox et al., 2005). FC analysis was conducted using the statistical parametric mapping (SPM) toolbox (Wellcome Department of Cognitive Neurology, Institute of Neurology, University College London; http://www.fil.ion.ucl.ac.uk/spm) within the Matlab computing environment (The Mathworks, Natick, Inc.). For details about the MRI protocol and MRI-fMRI data preprocessing see the dedicated paragraphs below and the Supporting Information section of the article.

A functional region of interest (ROI) representing the left angular gyrus node of the DMN was derived from a publicly available functional atlas (Shirer, Ryali, Rykhlevskaia, Menon, & Greicius, 2012) (for a description of the atlas see http://findlab.stanford.edu/functional_ROIs.html). A seed-to-voxel correlation-map was computed for each participant, thus obtaining a map of positively and negatively correlated voxels, respectively representing the DMN and TPN. Two independent investigators checked both FC maps and structural MRI data (i.e., T1-weighted images) in order to identify individual hotspots satisfying the following set of ad-hoc criteria: stimulation sites should be (i) as close as possible to the local maxima of the FC cluster identified as DMN-angular gyrus; (ii) being on the top of a cortical gyrus (avoiding sulci); (iii) represent the shortest perpendicular path connecting the stimulating TMS coil on the scalp and the cortex. Based on best judgment, the resulting set of coordinates was picked as DMN stimulation site in the parietal lobe (t^{DMN}). The same procedure was applied to the identification of the TPN stimulation site in the prefrontal region (t^{TPN}). However, given the individual variability in topography of left angular gyrus seed-based FC maps, additional criteria were introduced. t^{TPN} was defined as: (iv) a frontal lobe hotspot showing negative FC values with left angular gyrus; (v) not necessarily showing the strongest negative correlation whereas being the centroid of the (vi) widest negative correlation cluster, and also the (vii) farther apart from positively correlated nodes. This approach was thought to ensure the highest individualization of stimulation targets, meanwhile accounting for potential errors during neuronavigation (i.e., trial by trial coil displacement). As shown in Figure 1b, individualization of cortical stimulation

sites led to considerably different maps for each participant, strongly supporting the need for such approach when modulation of FC patterns is desired. Without such individualization and by using, for instance, coordinates derived from prior publications or from the international 10–20 EEG system, the vast majority of the participants would have been stimulated in the same region but on either negatively or positively connected spots, thus vanishing the effort of focusing on the negative correlation between DMN and TPN. Once optimal stimulation nodes were identified, target sites were loaded into the neuronavigation software (see Supporting Information Materials). Two participants did not display clear functional connectivity patterns between DMN and TPN, possibly due to movement artifacts, and were therefore excluded from the study (Supporting Information Figure S2).

2.5 | Test–retest reliability of TMS targets

Variability in FC patterns is expected both between participants and within each participant's when scanned multiple times over multiple days (Braun et al., 2012). The effort for individualization of fMRI targets might be vanished if resulting networks topographies do not show high levels of similarities across TMS visits. We computed FC maps for t^{TPN} and t^{DMN} using fMRI data collected on the day of targets definition (Week 1, Figure 1) and fMRI data collected before each ccPAS visit (Weeks 2–4, Figure 1). The maps were tested for similarity using paired t-tests (e.g., baseline vs. visit 2; baseline vs. visit 3). Moreover, individual stimulation sites for visit 2–3–4 were also identified and visualized against those defined on visit 1 (i.e., those used for ccPAS), providing a quantitative map showing the displacement between visit 1 and 2–3–4 targets (Figure 2).

2.6 | TMS and ccPAS parameters: Intensity, coil orientation, ISI

Cortico-cortical paired associative stimulation (ccPAS) was performed using a STM9000 magnetic stimulator (Ates-EBNeuro Ltd), connected to two 70 mm figure-8 coils. Individual resting motor-threshold (RMT) measurements were used to select stimulation intensity before each ccPAS visit, by using a module for electromyography (EMG) recording connected to the TMS stimulator. According to international guidelines (Rossini et al., 2015), RMT was determined for left motor cortex "hot spot", corresponding to the scalp location where single TMS pulses were able to evoke a motor responses (~50 μV as recorded using EMG) in the right first dorsal interosseous (FDI) muscle in at least 50% of 10 trials. EMG activity was measured using a recording and a ground electrode, with the active electrodes positioned over the belly of the FDI muscle, while the reference was placed over the metacarpophalangeal joint of the index finger. To stimulate left M1, the TMS coil was positioned at an angle of approximately 45° respect to the midline over the scalp location of the left FDI "hot spot" (~6 cm lateral and 3 cm anterior to the vertex in the EEG 10–20 system) to induce a posterior-to-anterior (PA) current flow.

Stimulation over the left angular gyrus (t^{DMN}) was done with the coil positioned with a 15° angle respect to the midline, according to previous studies (Koch et al., 2007, 2013; Veniero, Ponzo, & Koch, 2013) (see Figure 1e). Stimulation over the left frontal lobe (t^{TPN}) was

performed by keeping the coil at a 45° orientation respect to the midline. ccPAS consisted of 180 paired TMS pulses delivered every 5 s (0.2 Hz) over a period of 15 min. Inter Stimulus Intervals (ISI) varied across sessions: +10 ms ($t^{DMN} \rightarrow t^{TPN}$ condition), −10 ms ($t^{TPN} \rightarrow t^{DMN}$) and 0 ms ($t^{DMN} \leftrightarrow t^{TPN}$, control condition). The TMS pulse over the left angular gyrus preceded ($t^{DMN} \rightarrow t^{TPN}$), followed ($t^{TPN} \rightarrow t^{DMN}$), or coincided with ($t^{DMN} = t^{TPN}$) the one over the middle frontal gyrus. The three TMS conditions were performed across three different sessions over 3 weeks (Figure 1e). Stimulation was set to monophasic pulse. The conditioning stimulus (i.e., first TMS pulse) intensity was set at 90% of RMT, while the test stimulus (i.e., second TMS pulse) was applied at 120% RMT according to previous PAS studies in the motor system (Koch et al., 2013; Koganemaru, Mima, Nakatsuka, Ueki, Fukuyama, &, Domen, 2009).

2.7 | fMRI data acquisition and preprocessing

2.7.1 | Data acquisition

MRI data was acquired on a Philips Intera whole-body MRI scanner at the Le Scotte Hospital in Siena (Italy). Resting-state fMRI data included 178 volumes with 33 axial slices covering the whole brain, acquired via a T2 BOLD-sensitive multi-slice echo planar imaging (EPI) sequence (TR/TE = 2.5 s/32 ms; field of view = 22 cm; image matrix = 64×64; voxel size = $3.44 \times 3.44 \times 3.8$ mm^3; flip angle = 75°). Structural imaging was performed using a whole brain T1-weighted Fast Field Echo 1mm^3 sequence (TR/TE = 30/4.6 ms, field of view = 250 mm, matrix 256×256, flip angle = 30°, slice number = 150). T2-weighted Fluid Attenuated Inverse Recovery Images (FLAIR) were also acquired to assess participants white matter integrity. Participants were asked to lay in the scanner with their eyes open, stay still as much as possible and fixate a cross-air placed in front of them. They were provided with earplugs and particular care was taken to minimize head motion via vacuum cushions and custom-made padding.

2.8 | Task-fMRI data: Attention task

Given the novelty of the application of ccPAS over fronto-parietal fMRI networks, we considered the investigation of task-fMRI an additional exploratory aim of the study. By adopting a block design including rest and attention blocks, we predicted that ccPAS would modulate the switch between DMN and TPN occurring at the transition between the two brain states (i.e., rest, attention). If ccPAS was able to increase or decrease the association (i.e., connectivity) between DMN and TPN at rest, this might also result in a slower or faster transition between the two corresponding brain states (e.g., stronger deactivation of the DMN at the onset of the attention task blocks) supported by the two networks (rest → DMN; attention → ASN).

2.8.1 | Task description

Participants carried out a sustained attention task assessing their ability to direct attention to visual stimuli (i.e., geometric figures) presented in their visual field inside the MRI scanner, following work as reported in Tomasi, Ernst, Caparelli, and Chang (2006). Each participant performed two block-design fMRI runs (before and after ccPAS, see Figure 1e), composed by nine rest and nine active blocks. Each
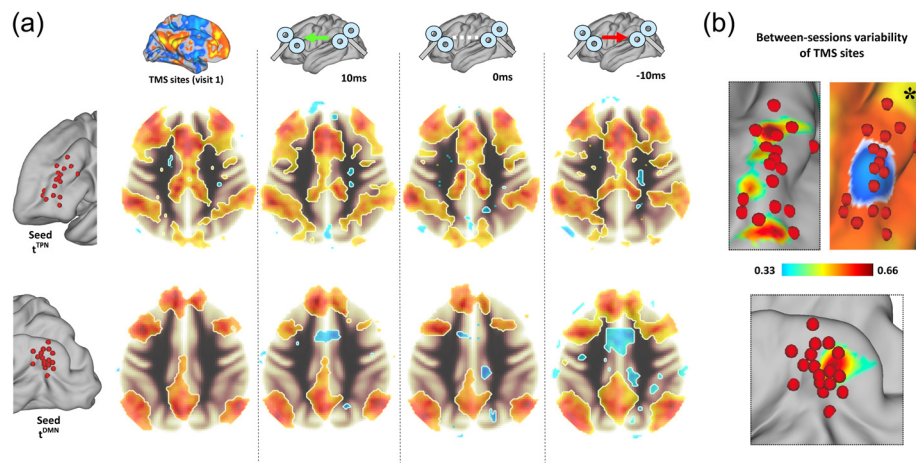
FIGURE 2 Reliability of TMS sites. (a) Group average maps of TPN (above) and DMN (below) are reported for each fMRI visit (left to right), showing the spatial similarity across maps obtained the day of TMS targets definition (Week 1) and the three ccPAS visits (Week 2–3–4). (b) Individual TMS targets were calculated for the first fMRI run of each ccPAS visit, and a quantitative displacement map across participants was calculated. Targets in the frontal lobe show high variability for participants with initial targets located at the superior and inferior boundary of the average cluster of negative correlation with the DMN (∗). As for the DMN, lower variability was observed [Color figure can be viewed at wileyonlinelibrary.com]

"active" block lasted for 50 s, with participants seeing a random selection of six different shapes (i.e., red dot, yellow star, green square, blue triangle, orange rhombus, pink heart), with the red dot stimuli being always present on the screen. Within each block, shapes alternated with an inter-stimulus interval (ISI) equals to 15 ± 10 s. The number of shapes presented in each run was kept low on purpose, trying to avoid engagement of memory processes which might possibly have an effect on DMN activity during "rest" blocks (i.e., rehearsal of previously seen stimuli; Chen et al., 2016). Participants kept their eyes open during rest block and were instructed to fixate the red dot. At the end of each fMRI run, participants were asked how many stimuli were being presented other than the red dot, with no instruction to specify which stimuli was specifically presented. This was intended to minimize the cumulative memory load of the task, focusing on mapping attention-related performance.

2.9 | Functional and effective connectivity analysis

2.9.1 | Regions of interest definition

Functional and effective connectivity analysis was based on individual spherical ROIs created for each participant. ROIs were 5 mm radius in size and located in correspondence of the t^{TPN} and t^{DMN} stimulation sites (see Figure 1 and Supporting Information Figure S1, red dots). Exact positioning was done by projecting the scalp location of the TMS pulse on the cortical surface; the spheres were then created in correspondence of the closest cortical gyrus. To ensure any misplacement and/or influence of signal from white matter or CSF, all the ROIs were masked using individual gray matter binary masks created during the brain segmentation procedure.

2.9.2 | Functional connectivity analysis

Functional connectivity (FC) was calculated by computing the Pearson product–moment correlation coefficient between the average BOLD time series extracted from each individual ROI and each remaining voxel in the brain. Seed-based FC maps were then compared using a repeated measures Analysis of Variance (rp-ANOVA) model, using a statistical threshold equal to $p < .001$ at single voxel level (False Discovery Correction, FDR) and $p < .01$ (Family Wise Error, FWE) (Worsley et al., 1996) for cluster-level correction. Analysis was done by testing the effect of two factors, "ISI" and "TIME," respectively representing the delay between TMS pulses (3 levels = +10 ms, −10 ms, 0 ms) and the different rs-fMRI runs acquired before and after ccPAS (3 levels = pre, post-5′, post-40′). When a main or interaction effect was observed, post-hoc tests were performed to highlight the specific contrast showing significant changes after ccPAS. Results were considered significant for a p value <.002 for F tests and p value <.016 for each t test performed separately. Age and gender were included as covariates in the analysis. Results of both FC and Task-fMRI analyses were visualized using the Connectome-Workbench software, applying the volume-to-surface scripts developed by the Human Connectome Project team. For reference see http:/www.humanconnectome.org/software/connectome-workbench.html.

2.9.3 | Directed information flow analysis

Given the supposedly directed nature of the inter-regional modulation elicited by ccPAS, the influence of each stimulated region over the rest of the brain was also tested by means of effective connectivity (EF) analysis (Friston, Moran, & Seth, 2013).

To assess the changes in the influence between t^{TPN} and t^{DMN} ROIs and the rest of the brain after TMS, the average BOLD time series extracted from individual 5 mm radius spheres were used to estimate effective connectivity (Deshpande & Hu, 2012; Friston et al., 2013; Roebroeck, Formisano, & Goebel, 2005). Specifically, A → B influence was estimated following the approach described in (Seth, Chorley, & Barnett, 2013), allowing to extract seed-to-brain voxel-wise maps representing so-called "directed information flow" (Barnett, Barrett, & Seth, 2017). The method applied here stem from Granger Causality (GC) analysis, and it is based on the concepts of predictability and precedence: variable A is said to modulate variable B if the

past behavior of A contains information that helps predict the future behavior of B over and above information already in the past of B. Importantly, this might allow to disentangle the differential effect of ccPAS delivered with opposite ISIs (A → B and B → A). In recent years, criticism about pairwise GC analysis has been growing (Smith, 2012; Barnett et al., 2017), leading to the development of newer approaches for information flow estimation such as the one implemented in the present investigation (Stokes & Purdon, 2017; Faes, Stramaglia, & Marinazzo, 2017; Seth et al., 2013). However, it must be also noticed that the nature of previous GC results has been questioned in the context of correlation studies, where effective connectivity has been linked to behavior. Instead, the present study might represent a proper context for directed information flow application, given the focus on region-to-region modulation of information flow, elicited by an external intervention with a specific "direction." Indeed, when testing the hypothesis that ccPAS over A → B might result in the modulation of the influence that A exerts on B, effective connectivity might actually be a more appropriate tool than functional connectivity.

Similar to FC analysis, the analysis produced seed-based, voxel-wise maps for each ROI, allowing to build rp-ANOVA models as those described above. An example of resulting map is visible in Figure 3a, highlighting the expected strong positive modulation played by the left angular gyrus (i.e., t^{DMN}) over other nodes of the same network (DMN), while weaker modulation is present over the rest of the brain (i.e. strong within network synchrony and predictability among nodes of the same network). Positive modulation represents the influence of one area toward another, which in fMRI terms can be seen as a positive link between increase in BOLD response in region A (i.e. t^{DMN}) triggering an increase of BOLD response in other connected regions (e.g. B, t^{TPN}). Seed-based GC maps were compared using a rp-ANOVA with a statistical threshold equals to $p < .001$ at single voxel level (FDR) and $p < .01$ (FWE) for cluster-level correction. Analysis was done by testing the effect of two factors, "ISI" and "TIME," respectively representing the delay between TMS pulses (3 levels = +10 ms, −10 ms, 0 ms) and the different rs-fMRI runs acquired before and after ccPAS (3 levels = pre, post-5′, post-40′). When a main or interaction effect was observed, post-hoc tests were performed to highlight the specific contrast showing significant changes after ccPAS.

2.10 | Task-fMRI data analysis

Analysis was performed using a general linear model (GLM), as implemented in SPM12. Separate regressors were built for each condition and convolved with the hemodynamic response function (HRF). A random effect second-level analysis was then calculated for each condition. Results were shown for each contrast (attention > rest; rest > attention) using a threshold equals to $p < .001$ at single voxel level (FDR) and $p < .01$ (FWE) for cluster-level correction. The GLM model was a full factorial $2 \times 3 \times 2$ repeated measures ANOVA design, including factors "TIME" (two levels = Pre- and Post- ccPAS), "ISI" (three levels = 0 ms, +10 ms, −10 ms) and "BRAIN STATE" (two levels = Attention, Rest). Moreover, to disentangle significant main effects and interactions of interest, separate analyses were carried out on single factors (e.g., TIME) by focusing on each level separately.

Results were considered significant for a p value <.003 for F tests and p value <.016 for t tests. Results are reported in MNI space.

Given the continuous switching between an active and passive state during the task, and the role played by DMN-TPN dynamics in determine the efficacy of such switch (Andrews-Hanna, 2012; Raichle, 2015), analyses were also performed on three incremental time windows (i.e., sub-blocks), focusing on the changes in activation patterns right after the switch between active → rest and rest → active (i.e., analysis on the first 10 s of each block; 10 s), over the first 30 s after the switch and during the entire block, i.e. 50 s. This allowed to look at the potential effect of ccPAS on transient reconfiguration involving the interplay of the two networks, most likely happening at the transition between task conditions—and brain state—rather than for the entire duration of each block. Separate statistical models were built using HRF convolved fMRI data limited by the windows of interest. Analysis and corresponding results are shown in Figure 5b.

3 | RESULTS

3.1 | Test–retest of TMS targets across sessions

Figure 2a shows the FC maps for t^{TPN} and t^{DMN} computed using fMRI data collected on the day of targets definition (visit 1), and fMRI data collected before each ccPAS visit (visit 2–4). The maps were tested for similarity using paired t-tests (e.g. baseline vs. visit 2; baseline vs. visit 3; $p < .05$ with false discovery correction, FDR), with no significant differences detected for any comparison (critical two-sided $t = 3.46$, $p = .001$ FDR at voxel-level, $p = .01$ FWE at cluster level). Moreover, we looked at the position of each TMS targets when defined using each fMRI datasets collected on visit 1–4. Highest variability was observed for t^{TPN} targets located at the superior and inferior boundary of the average cluster of negative correlation with the DMN (Figure 2b). Lower variability was observed for t^{DMN} targets, with major differences for participants with more posterior initial TMS targets. Overall, the magnitude of the displacement suggested satisfying reproducibility levels for both t^{TPN} and t^{DMN}, with stronger importance of individualizing TMS sites for stimulation over prefrontal regions.

3.2 | Modulation of inter-regional FC

The longitudinal comparison of $t^{DMN} \rightarrow t^{TPN}$ and $t^{DMN} = t^{TPN}$ conditions revealed a main effect for TIME ($F_{[2,13]} = 3.05$, $p = .002$, $\eta^2 = 0.058$) and ISI ($F_{[2,13]} = 2.87$, $p = .004$, $\eta^2 = 0.049$), as well as a significant TIME*ISI interaction for rs-fMRI data collected right after ccPAS (i.e., within 5 min after TMS, see Figure 1e) ($F_{[2,13]} = 2.64$, $p = .007$, $\eta^2 = 0.045$).

Post-hoc tests were used to disentangle the main effects and interaction, showing a significant change in FC right after STDP-inducing ccPAS with an ISI of +10 ms ($t_{[16]} = 3.27$, $p = .008$, Cohen's $d = 0.45$; Figure 3a; MNI coordinates = −32, 48, 30). The effect represented a decrease in the negative correlation between t^{DMN} and a cluster of voxels resembling t^{TPN} (Figure 3a). The same pattern was observed for $t^{DMN} \rightarrow t^{TPN}$ pairwise connectivity based on individual stimulation sites, that is, using 5 mm radius spheres as regions of interest ($t_{[2,13]} = 3.69$, $p < .007$, Cohen's $d = 0.48$; Figure 3b,c). Interestingly, changes after
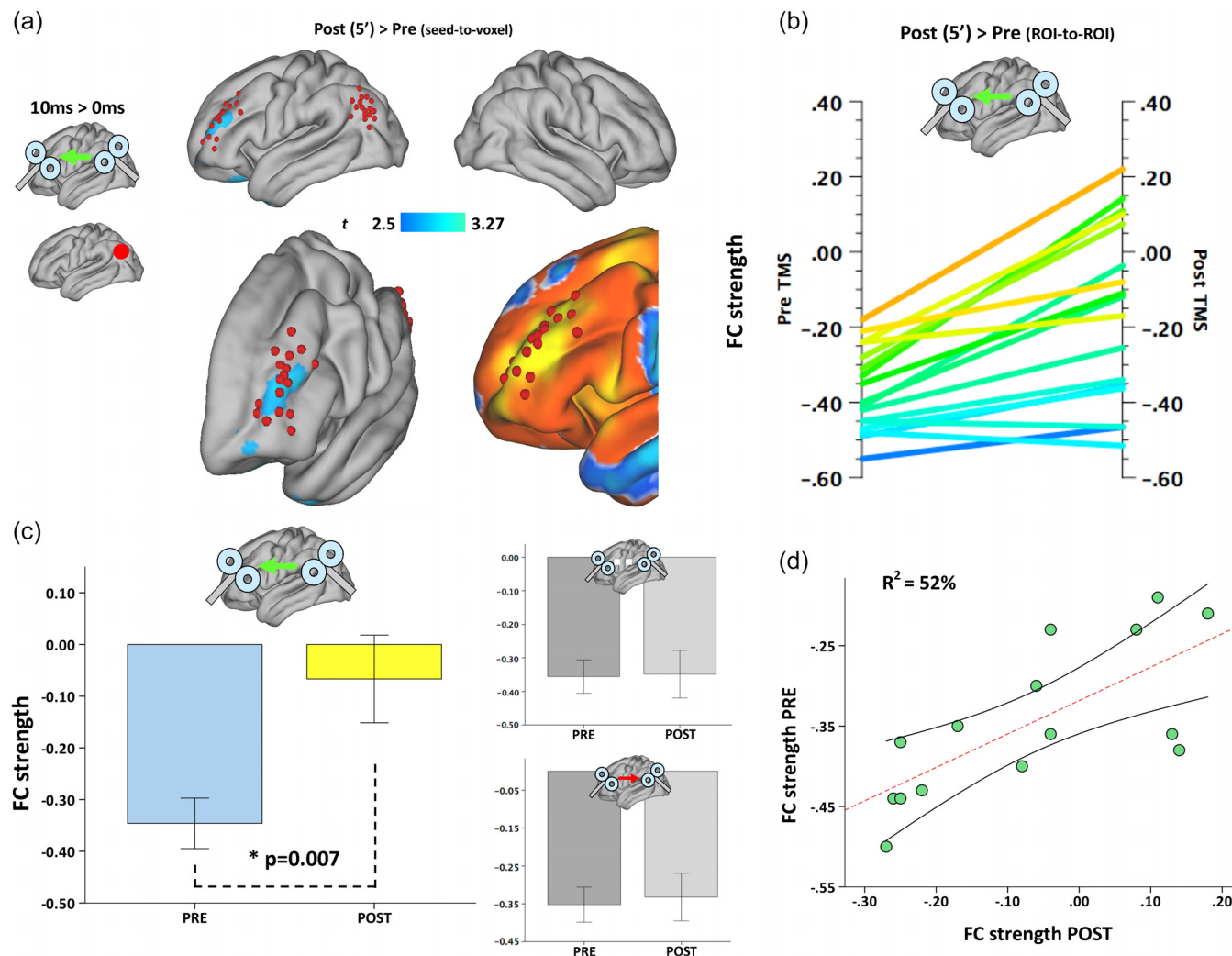
FIGURE 3 Modulation of pairwise functional connectivity. (a) Group-level, seed-to-voxel analysis unveiled a significant modulation of the coupling between t^{DMN} and a cluster resembling individual t^{TPN} targets (red dot = seed region). (b,c) analysis of individual t^{DMN} and t^{TPN} ROIs after $t^{DMN} \rightarrow t^{TPN}$ compared with $t^{DMN} = t^{TPN}$ revealed a significant decrease in pairwise negative FC strength, with ~33% of subjects reversing their initial negative correlation (b,c show individual pre-/post-TMS FC values and pooled data, respectively; lines in (b) are color-coded [blue = lowest value, yellow = highest value] according to pre-TMS FC strength). (d) Participants with stronger negative FC before stimulation showed a weaker modulation following ccPAS, whereas weaker negative FC before stimulation predicted stronger modulatory effects [Color figure can be viewed at wileyonlinelibrary.com]

$t^{DMN} \rightarrow t^{TPN}$ also correlated with individual baseline FC strength (i.e., pre-ccPAS), with a stronger modulation of FC observed in subjects with weaker negative FC values at baseline (ISI = +10 ms, $p = .003$, $R^2 = 52\%$; ISI = −10 ms, $p = .36$, $R^2 = 2.9\%$; ISI = 0 ms, $p = .48$, $R^2 = 1.7\%$) (Figure 3d). No other significant changes were observed in cortical or subcortical regions in both hemispheres.

Additionally, a strengthening of spontaneous connectivity within the nodes of the DMN was also found following $t^{DMN} \leftrightarrow t^{TPN}$ ccPAS (i.e., ISI = +10 ms; 5′ after ccPAS) ($t_{[16]} = 2.04$, $p = .015$, Cohen's $d = 0.31$; MNI = −24, −22, −24) (Figure 4a). This is in agreement with prior observation of increased cortico-subcortical coupling following single target TMS over the left parietal lobe, with cascade effects in medial temporal lobe structures including the hippocampus (Eldaief et al., 2011; Wang et al., 2014).

Finally, increased positive connectivity between t^{DMN} and medial-prefrontal nodes of the DMN ($t_{[16]} = 2.7$, $p = .012$, Cohen's $d = 0.35$; MNI = −10, 44, 44; Figure 4b), and between t^{TPN} and the same medial

prefrontal nodes of the DMN, were also observed in resting-state fMRI data collected 5′ after ccPAS with ISI = −10 ms ($t^{TPN} \rightarrow t^{DMN}$) ($t_{[16]} = −2.16$, $p = .019$, Cohen's $d = 0.33$; MNI = −10, −52, 26; Figure 4c). This suggests a general pattern of higher responsiveness to TMS for medial DMN structures (i.e., precuneus, posterior cingulate cortex, medial prefrontal cortex), when pulses are delivered either on the parietal or the prefrontal target. Interestingly, such DMN-related response also mimicked the results of task-fMRI data, where changes in the switch between Rest and Task blocks were observed in the activity of medial DMN structures (see next paragraph, Figure 5a,b). No significant effects were observed at delayed fMRI recording (40′ after ccPAS).

3.3 | Changes in evoked activity

Results are shown in Figure 5a,b. Detailed statistical results for each comparison, including "Task > Rest" and "Rest > Task" contrasts averaged across factors "TIME" and "ISI," are reported in Supporting Information
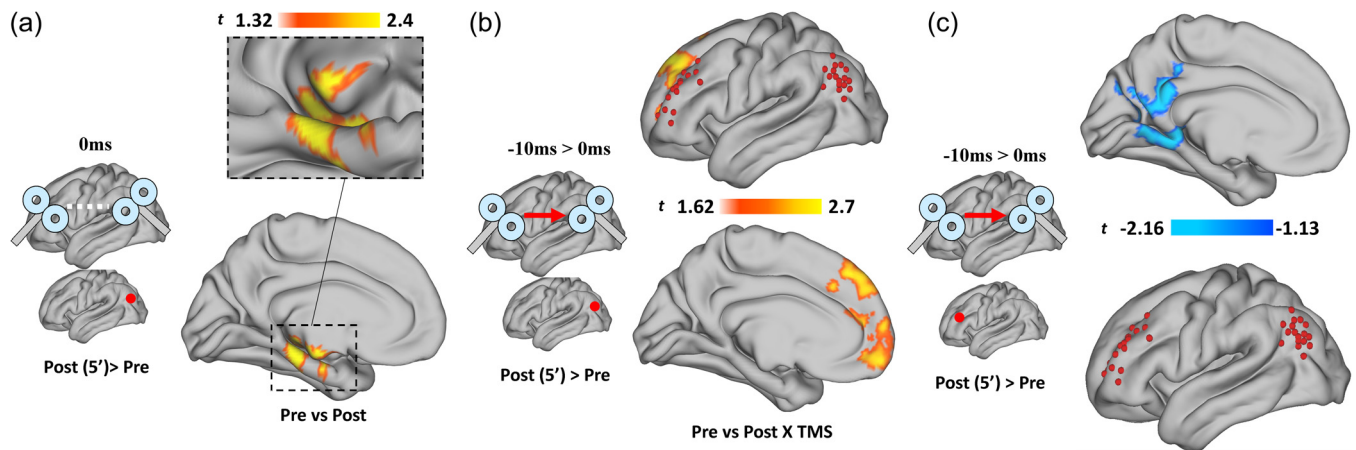
FIGURE 4 Within network effects. (a,b) modulation of FC was also present for $t^{DMN} = t^{TPN}$ and $t^{DMN} \rightarrow t^{TPN}$, but limited to changes in within-DMN connectivity. TMS delivered simultaneously on both t^{DMN} and t^{TPN} (i.e., the "control" ISI not inducing STDP) elicited an increase in t^{DMN} connectivity with the ipsilateral parahippocampal gyrus (a, red dot = seed region), while $t^{TPN} \rightarrow t^{DMN}$ modulated t^{DMN} and t^{TPN} connectivity with dorso-medial and ventro-medial DMN regions (b,c) [Color figure can be viewed at wileyonlinelibrary.com]

Table S1. The activation patterns during Task and Rest conditions are displayed in Figure 5a, with the expected activation of nodes of the TPN (including the anterior salience network, ASN; [Dosenbach et al., 2007], and dorsal attention network, DAN [Corbetta & Shulman, 2002]) during the sustained attention task. Importantly, task activations in the left middle frontal gyrus overlapped with the cluster of t^{TPN} sites, suggesting that frontal lobe ccPAS was successfully targeting a relevant region for attention-related dynamics.

Given the hypothesized modulation of the switch between DMN and TPN during the transition between rest/attention blocks, the analysis of evoked activity was performed across three different time windows, capturing evoked activity within the first 10s, 30s and 50s after rest/task

blocks onset (50 s = entire block; see Section 2 for more details on the task-fMRI analysis). Significant effects for TIME ($F_{[2,13]} = 3.15$, $p = .018$, Cohen's $d = 0.26$), ISI ($F_{[2,13]} = 3.42$, $p = .0031$, Cohen's $d = 0.28$), and BRAIN STATE ($F_{[2,13]} = 3.04$, $p = .024$, Cohen's $d = 0.26$) were found. Significant interactions were found, with a significant difference in BOLD response for $t^{DMN} \rightarrow t^{TPN}$ and $t^{TPN} \rightarrow t^{DMN}$ as compared with $t^{DMN} = t^{TPN}$ in Rest blocks (see Figure 3e), suggesting a stronger deactivation of attention-related regions and a stronger activation of DMN nodes after ccPAS. Specifically, $t^{DMN} \rightarrow t^{TPN}$ induced increased activation of medial prefrontal DMN structures especially over the first 10 s (+10 ms > 0 ms = [0–10 s; $t_{(16)} = 3.45$, $p = .007$, Cohen's $d = 0.30$; MNI = 6, −56, 25]; [0–30 s; $t_{(16)} = 3.19$, $p = .017$, Cohen's $d = 0.27$;
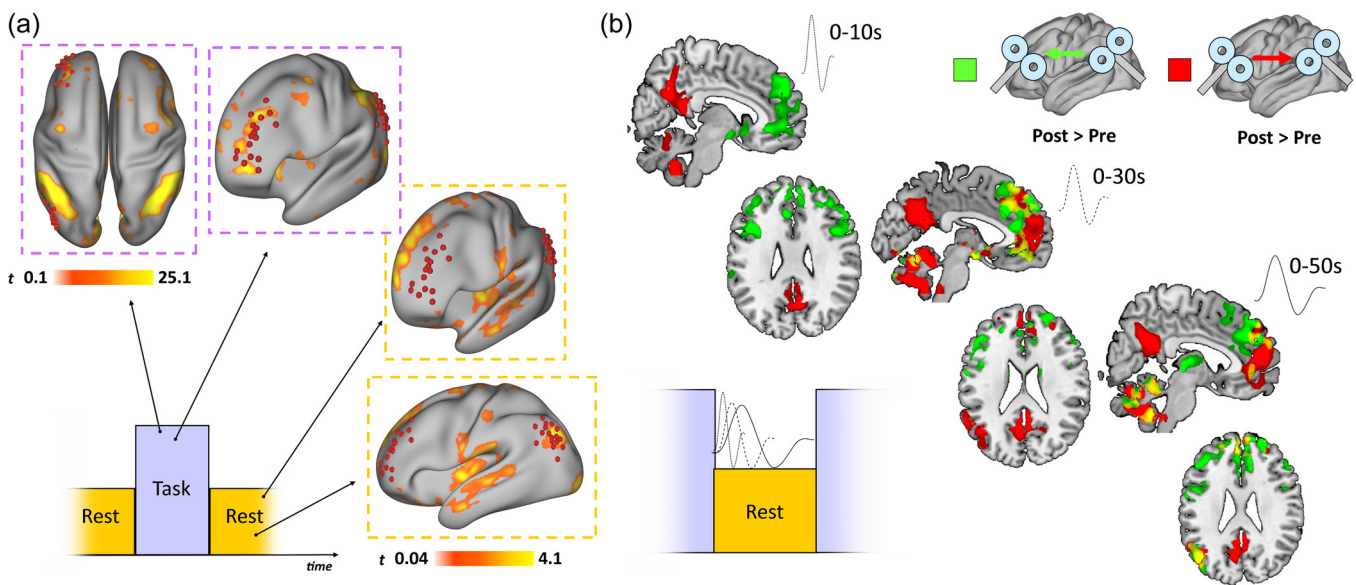

FIGURE 5 Task-fMRI modulation. (a) As expected, the attention task elicits network-specific activation patterns resembling TPN and DMN activity. (b) Two patterns of increased BOLD response were observed after $t^{DMN} \rightarrow t^{TPN}$ and $t^{TPN} \rightarrow t^{DMN}$, with a time-dependent increase in, respectively, ventro-medial and dorso-medial DMN nodes activity at the onset of rest blocks (i.e., first 10 s). Increased engagement of additional DMN nodes such as the left angular gyrus (corresponding to t^{DMN}) was observed over time within each block (i.e., 30 and 50 s), with no significant changes observed for the contralateral angular gyrus. Note: Color bars report z-transformed FC values [Color figure can be viewed at wileyonlinelibrary.com]

MNI = 8, −46, 30]; [0–50 s; $t_{(16)}$ = 3.16 p = .026, Cohen's d = 0.24; MNI = 8, −48, 28]) (Figure 5b, green), while $t^{TPN} \rightarrow t^{DMN}$ induced a mirrored pattern, with higher activation of posterior medial DMN structures (−10 ms > 0 ms = [0–10 s; $t_{(16)}$ = 2.93, p = .023, Cohen's d = 0.21; MNI = 4, −59, 30]; [0–30 s; $t_{(16)}$ = 2.85, p = .029, Cohen's d = 0.20; MNI = 4, 50, 24]; [0–50 s; $t_{(16)}$ = 2.80, p = .033, Cohen's d = 0.21; MNI = 4, 40, 30] (Figure 5b, red).

3.4 | Changes in information flow

Voxel-wise maps representing the EC between a seed region and the rest of the brain were computed by using t^{DMN} and t^{TPN} as seeds (Figure 6a) and compared across factors TIME and ISI. Without using regions of interest other than the two stimulation sites, the analysis was thought to provide an unbiased map of changes in information flow in the entire brain with respect to each TMS target. As shown in Figure 6b and similar to what observed at the FC analysis, a significant effect for TIME ($F_{[2,13]}$ = 3.31, p = .004, η^2 = 0.048) and ISI ($F_{[2,13]}$ = 2.56, p = .008, η^2 = 0.042) and a significant TIME*ISI interaction for rs-fMRI data collected right after ccPAS ($F_{[2,13]}$ = 2.33, p = .009, η^2 = 0.039) were found. The interaction was related to the comparison of $t^{DMN} \rightarrow t^{TPN}$ vs. $t^{DMN} = t^{TPN}$ ($t_{(16)}$ = 2.18, p = .017, Cohen's d = 0.31; MNI = −38, 42, 26), representing a selective increase in the modulation exerted by t^{DMN} over a cluster of voxels resembling t^{TPN} (Figure 6b). Crucially, control analyses showed no modulation of t^{DMN} and t^{TPN} influence over other cortical/subcortical brain regions after TMS (e.g., visual, auditory,

and motor cortices; Supporting Information Figure S3), suggesting spatial specificity for ccPAS effects. No significant effects were observed after $t^{TPN} \rightarrow t^{DMN}$ condition.

4 | DISCUSSION

Results support the possibility of manipulating network-to-network functional connectivity patterns by means of individualized noninvasive brain stimulation. We showed a modulation of spontaneous and evoked activity between two distinct intrinsic networks, with a significant reduction of their spontaneous negative correlation as well as changes in activation patterns during an attention task. Targeted interventions aimed at selectively modifying resting-state fMRI internetwork coupling by means of multi-site stimulation have not been described yet, with the only evidence available in humans being related to the modulation of single network dynamics via stimulation of one cortical target (Eldaief et al., 2011; Halko et al., 2014; Wang et al., 2014; Gratton et al., 2013). The possibility of selectively target nodes of two distinct networks, in the frame of an established STDP-inducing paradigm, might help gaining deeper understanding on brain-behavior causal relations.

Evidence in the motor and visual cortices suggest how ccPAS parameters, such as inter-stimulus timing (in the order of a few milliseconds) and directionality of the two pulses (A → B vs. B → A), play a crucial role into enabling the occurrence of STDP by matching or not
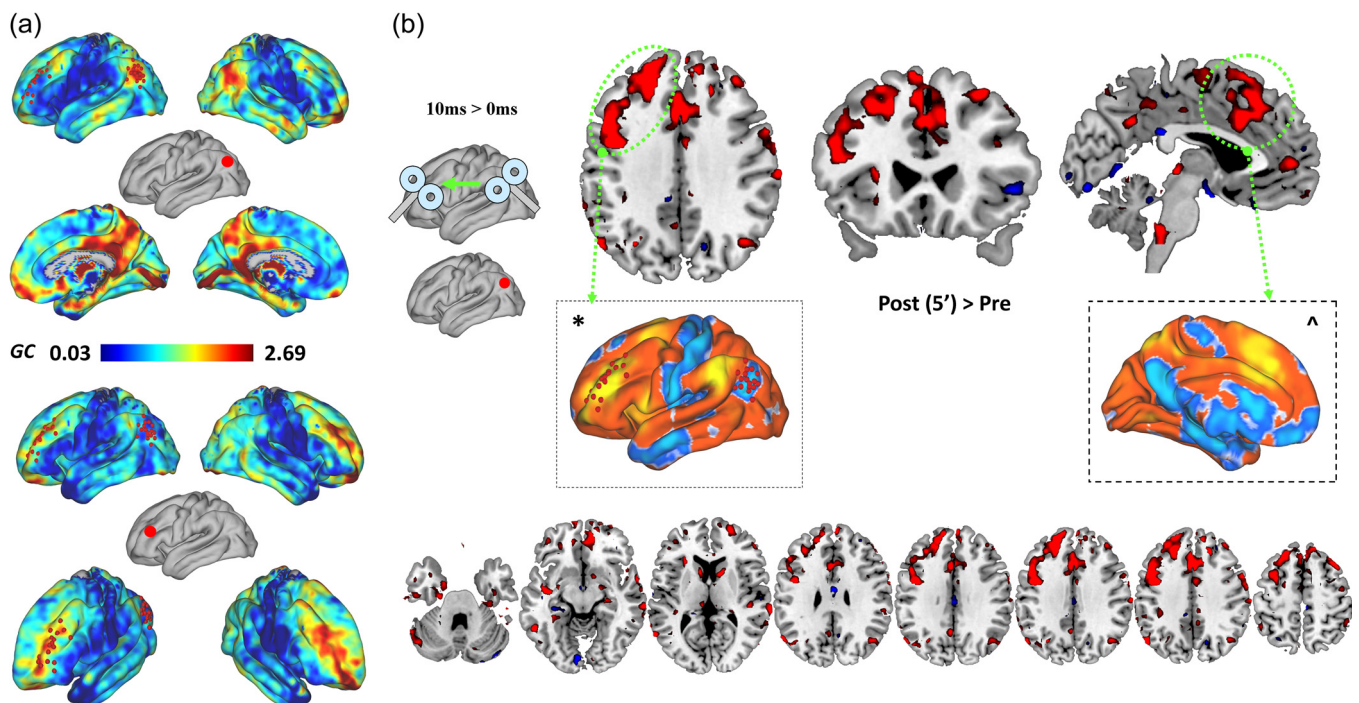

FIGURE 6 Modulation of effective connectivity. (a) Effective connectivity (EC) analysis of t^{DMN} activity before stimulation revealed a group-level pattern of seed-to-voxel effective connectivity mostly affecting the dorsal DMN (above), with weak modulation of t^{TPN} sites at baseline (red dot = seed region). The EC profile of t^{TPN} showed similar results (below), with greater modulation of within-network connectivity, mostly involving TPN nodes in the contralateral prefrontal cortex. (b) EC changes after $t^{DMN} \rightarrow t^{TPN}$ included increased modulation exerted by t^{DMN} over a cluster of voxels resembling t^{TPN} (*) and the anterior cingulate cortex (^), both nodes of the TPN. Axial views of the significant cluster modulated by t^{DMN} after TMS are also shown. Modulation of EC was limited to TPN/ASN nodes, with no effects over other cortical or subcortical regions (see Supporting Information Figure S3). Note: Color bar reports z-transformed GC values [Color figure can be viewed at wileyonlinelibrary.com]

spontaneous inter-regional activity (Casula et al., 2016; Koch et al., 2013; Rizzo et al., 2009; Veniero et al., 2013). In the present experiment we adopted a delay successfully applied to two left fronto-parietal regions in a previous TMS-EEG study (Casula et al., 2016), and also consistent with the lower bound of proposed propagation velocity of cortico-cortical associative fibers (Massimini, 2004; Nunez & Srinivasan, 2014). However, it cannot be excluded that other delays might be more efficient in inducing longer after effects and should be systematically tested in dedicated experiments, especially taking into account individualized information derived from, for example, connectivity of white matter tracts (Jbabdi, Sotiropoulos, Haber, Van Essen, & Behrens, 2015) or TMS-EEG recordings (Casali et al., 2013). As for the direction of modulation elicited by ccPAS, parieto-frontal ccPAS seems more successful in eliciting changes in DMN-TPN interplay. This scenario is also corroborated by the results of the directed information flow analysis, showing a selective modulation of t^{DMN} effective connectivity patterns and no significant effects for t^{TPN}. The effect of ccPAS on functional connectivity might be subjected to brain state-related effects: being TMS performed during "resting-state," regions composing the DMN might be intrinsically more responsive to stimulation given their higher activation during rest; regions of the TPN might be instead less active at rest and could benefit more from TMS performed during a task. This might affect the likelihood of inducing STDP and its directionality (e.g., with stronger responsiveness over t^{DMN} as compared with t^{TPN} for +10 ms and 0 ms ccPAS conditions where DMN was receiving the conditioning pulse), but also explain why t^{DMN} showed significant modulation of its connectivity after zero-lag ccPAS ($t^{DMN} = t^{TPN}$). As suggested for the definition of optimal ISI, TMS-EEG recording could be used to extract inter-regional co-modulation indexes such as directed transfer entropy (Wibral, Vicente, & Lindner, 2014; Vicente, Wibral, Lindner, & Pipa, 2011), guiding the definition of hypotheses in future studies. Finally, the impact of brain state should be also tested, by testing different behavioral states during stimulation (e.g., working memory task, attention task, rest).

Previous evidence has suggested the value of using resting-state fMRI information to guide TMS targets selection (Wang et al., 2014). Our data support the need of individualizing stimulation targets on the basis of network connectivity, showing high individual variability in TMS targets for both the parietal and prefrontal nodes. As visible in Figure 1b–d and Supporting Information Figure S1, while the left angular gyrus node of the DMN roughly matches previously published group-average network maps (Shirer et al., 2012; Yeo et al., 2011), individual TMS sites in the frontal lobe show high spatial variability in our sample, possibly reflecting the heterogeneity of frontal functions and structural subdivisions along the anterior–posterior axis (Thiebaut de Schotten et al., 2017; Nee & D'Esposito, 2016). This suggests that a target identification procedure based on group-average rs-fMRI networks maps would have actually led to incorrect estimation of the hotspot for stronger negative correlation in around 25% of the participants. The implementation of connectivity-based targeting approaches has probably significantly contributed to achieve the connectivity modulation observed in our data, suggesting the need for a systematic comparison of options for target selection based on other approaches including graph-theory or effective connectivity. The latter could also allow defining the best stimulation "direction", pointing toward a pre-existing hierarchy of network-to-network influence that

might be leveraged to amplify ccPAS effects (Spreng, Sepulcre, Turner, Stevens, & Schacter, 2013; Zhou et al., 2018).

Apart from the clinical and cognitive relevance of DMN-TPN connectivity, the selection of targets belonging to two negatively correlated networks instead of two positively correlated nodes of the same network (e.g., left and right angular gyrus nodes of the DMN), was aimed at limiting the impact of within-network resonance effects observed in the case of TMS over one single region/network (Eldaief et al., 2011; Wang et al., 2014). Moreover, the stimulation over two positively coupled oscillators might also result in smaller, less detectable effects due to ceiling effects, given the stronger connectivity characterizing positive functional connections in the human brain as compared with negative ones (Fox et al., 2005). Successful application of ccPAS on positively correlated regions might require the selection of a network with low dimensionality and nodes with low nodal degree (Sporns, 2014).

Regardless of the associative, plasticity-inducing nature of the TMS protocol, changes in within-network connectivity were also observed (see Figure 4a), mimicking previously published fMRI findings based on TMS delivered over the same DMN node (Eldaief et al., 2011). Interestingly, the implementation of a 0 ms ccPAS condition allowed to control for such within-network effects, by regressing out local TMS effects. Future studies should validate this approach based on a not-associative PAS condition as compared with a nonphysiological ISI (e.g., 500 ms; Johnen et al., 2015) or sham stimulation.

As for task-fMRI data, a transient enhancement of the switching between DMN-TPN was observed for STDP-inducing ISI, with no effects during simultaneous t^{DMN}–t^{TPN} stimulation. This suggests that ccPAS with STDP-inducing ISI (i.e., +10 ms, −10 ms) is able to modulate physiological deactivations during cognitive processing. Interestingly, a differential deactivation pattern followed ccPAS at +10 ms and −10 ms, with, respectively, a stronger post-stimulation activity in prefrontal (medial prefrontal gyrus, anterior cingulate cortex, middle frontal gyrus) and parietal (precuneus, posterior cingulate cortex) nodes of the DMN, especially during the first 10 s of Rest blocks. This might reflect the "directionality" of ccPAS at +10 ms and −10 ms (parieto-frontal vs. fronto-parietal, respectively), somehow mimicking the previously observed increase in activity at the receiving end of the network in ccPAS experiments on the motor system (i.e., increased activity in "B" after $t^A \rightarrow t^B$) (Casula et al., 2016; Koch et al., 2013). Interestingly, the analysis of BOLD response highlighted a pattern of progressively increased response in the same nodes of the DMN as derived from the rs-fMRI analysis (Figure 4a–c). Increased task-fMRI deactivation was observed for both ventral and dorsal DMN nodes with the exception of the right angular gyrus, which also did not show modulation at the resting-state FC analysis (Figure 5a). This supports the suggested similarity in the spatial localization of spontaneous and evoked fMRI activity patterns in humans (Tavor et al., 2016), with ccPAS effects on resting-state activity possibly resonating on (i.e. "constraining") activation patterns. Future investigations should test for the effect on more challenging attention tasks, including a more extensive attention performance assessment performed outside the MRI scanner before and after stimulation. Additionally, given the role of DMN in mind wandering (Andrews-Hanna, 2012; Raichle, 2015), potential modulation of spontaneous mentation should also be

monitored using validated measures (e.g., task-unrelated thoughts task, TUT; Axelrod, Rees, Lavidor, & Bar, 2015; Christoff, Gordon, Smallwood, Smith, & Schooler, 2009).

The individual response to PAS in the present study has also shown strong baseline-dependent properties, a phenomenon observed in previous NIBS studies (Lustenberger et al., 2016; Tseng et al., 2012). The notion that the same principle might apply to the modulation of inter-regional/inter-networks dynamics is novel and intriguing. However, while LTP processes have been shown to follow similar baseline-dependent modulation (the concept of "rich getting richer, poor getting poorer"; Turrigiano, 2008; Zheng, Dimitrakakis, & Triesch, 2013), the present data offer insight on potentially different scenarios that might apply to negatively coupled BOLD fMRI oscillations. In the present study, increased $t^{DMN} \rightarrow t^{TPN}$ coupling via ccPAS was mostly due to modulation of weak baseline functional connectivity (Figure 2b), while milder effects were observed in participants with stronger negative baseline FC. Based on LTP mechanisms, ccPAS is supposed to strengthen association between regions, making the targeting of two negatively correlated regions a scenario where a significant modulation might actually signify reversing spontaneous dynamics. The fact that weakly associated regions display more responsiveness to stimulation is intuitive, and in line with the differential resilience to perturbation observed in strongly or weakly connected nodes of complex networks (Madeo, Talarico, Pascual-Leone, Mocenni, & Santarnecchi, 2017; Achard & Bullmore, 2007; Santarnecchi, Rossi, & Rossi, 2015). Moreover, homeostatic plasticity processes might also play a role, more effectively counteracting the destabilizing influence of PAS-induced synaptic plasticity when stronger correlations are present (Karabanov et al., 2015). Whether ccPAS at higher stimulation intensity might induce detectable after effects even in strongly positively connected networks should also be tested.

Homeostatic plasticity might be called into question also to explain the short-lasting effect observed for ccPAS protocols implemented in the present study, with null effects on brain connectivity observed at the delayed fMRI acquisition. This might be due to the experimental design, which included interleaved tasks and resting-state fMRI acquisition blocks. By requiring participants to actively engage in a cognitive task which presumably requires activation of additional brain regions with respect to those modulated by ccPAS (e.g. t^{DMN} and t^{TPN} in the contralateral hemisphere), we might have possibly weakened the transient modulation of $t^{DMN} \leftrightarrow t^{TPN}$ interplay generated by TMS. Moreover, the present investigation only considered exposure to a single ccPAS session, while the cumulative effect of repeated TMS sessions seems crucial for the modulation of within-network connectivity (Wang et al., 2014), a principle that likely applies to between-networks dynamics as well.

A few additional limitations of the study should be pointed out. We did individualize the stimulation targets based on resting-state fMRI patterns, and checked for the reliability of targets across sessions. Ideally, targets should be defined the same day of stimulation, a procedure which however cannot happen in real time and will always have to account for changes in connectivity values happening between the fMRI and TMS session. Secondly, while the targets were fairly consistent for left angular gyrus node of the DMN, variability was present in the prefrontal lobe. This could have impacted the individual response to TMS across participants given that different regions of the prefrontal cortex might respond differently to TMS, or require a slightly different ISI depending on different target-to-target distance or structural connectivity between targets. Individualization of ISI based on these parameters should be considered.

5 | CONCLUSION

Overall, results point to the possibility of modulating the spontaneous interplay between two intrinsic fMRI networks, with potential effects also during cognitive processing. This might constitute the background for future neuromodulatory interventions aimed at probing the role of specific brain functional connections, and potentially counteract altered connectivity patterns documented in physiological aging as well as in neurological and psychiatric conditions.

CONFLICT OF INTEREST

The authors declare that they have no conflicts of interest.

ORCID

Emiliano Santarnecchi https://orcid.org/0000-0002-6533-7427
Giulia Sprugnoli https://orcid.org/0000-0003-4621-9537
Simone Rossi https://orcid.org/0000-0001-6697-9459

REFERENCES

Abbott, L. F., & Nelson, S. B. (2000). Synaptic plasticity: Taming the beast. *Nature Neuroscience*, 3(Suppl), 1178–1183.

Achard, S., & Bullmore, E. (2007). Efficiency and cost of economical brain functional networks. *PLoS Computational Biology*, *3*, e17.

Adelstein, J. S., Shehzad, Z., Mennes, M., Deyoung, C. G., Zuo, X. N., Kelly, C., ... Milham, M. P. (2011). Personality is reflected in the brain's intrinsic functional architecture. *PLoS One*, *6*, e27633.

Altamura, M., Fazio, L., De, S. M., Petito, A., Blasi, G., Taurisano, P., ... Bertolino, A. (2012). Abnormal functional motor lateralization in healthy siblings of patients with schizophrenia. *Psychiatry Research*, *203*, 54–60.

Anderson, J. S., Druzgal, T. J., Froehlich, A., DuBray, M. B., Lange, N., Alexander, A. L., ... Lainhart, J. E. (2011). Decreased interhemispheric functional connectivity in autism. *Cerebral Cortex*, *21*, 1134–1146.

Andrews-Hanna, J. R. (2012). The brain's default network and its adaptive role in internal mentation. *The Neuroscientist*, *18*, 251–270.

Arai, N., Muller-Dahlhaus, F., Murakami, T., Bliem, B., Lu, M. K., Ugawa, Y., & Ziemann, U. (2011). State-dependent and timing-dependent bidirectional associative plasticity in the human SMA-M1 network. *The Journal of Neuroscience*, *31*, 15376–15383.

Axelrod, V., Rees, G., Lavidor, M., & Bar, M. (2015). Increasing propensity to mind-wander with transcranial direct current stimulation. *Proceedings of the National Academy of Sciences*, *112*, 3314–3319.

Barnett, L., Barrett, A. B., & Seth, A. K. (2017). Reply to Stokes and Purdon: A study of problems encountered in Granger causality analysis from a neuroscience perspective. ArXiv170808001 Stat. http://arxiv.org/abs/1708.08001

Boes, A. D., Prasad, S., Liu, H., Liu, Q., Pascual-Leone, A., Caviness, V. S., & Fox, M. D. (2015). Network localization of neurological symptoms from focal brain lesions. *Brain: A Journal of Neurology*, *138*, 3061–3075.

Braun, U., Plichta, M. M., Esslinger, C., Sauer, C., Haddad, L., Grimm, O., ... Meyer-Lindenberg, A. (2012). Test–retest reliability of resting-state connectivity network characteristics using fMRI and graph theoretical measures. *NeuroImage*, *59*, 1404–1412.

Buch, E. R., Johnen, V. M., Nelissen, N., O'Shea, J., & Rushworth, M. F. (2011). Noninvasive associative plasticity induction in a corticocortical pathway of the human brain. *The Journal of Neuroscience*, *31*, 17669–17679.

Casali, A. G., Gosseries, O., Rosanova, M., Boly, M., Sarasso, S., Casali, K. R., ... Massimini, M. (2013). A theoretically based index of consciousness independent of sensory processing and behavior. *Science Translational Medicine*, *5*, 198ra105–198ra105.

Casula, E. P., Pellicciari, M. C., Picazio, S., Caltagirone, C., & Koch, G. (2016). Spike-timing-dependent plasticity in the human dorso-lateral prefrontal cortex. *NeuroImage*, *143*, 204–213.

Chen, J., Leong, Y. C., Honey, C. J., Yong, C. H., Norman, K. A., & Hasson, U. (2016). Shared memories reveal shared structure in neural activity across individuals. *Nature Neuroscience*, *20*, 115–125.

Christoff, K., Gordon, A. M., Smallwood, J., Smith, R., & Schooler, J. W. (2009). Experience sampling during fMRI reveals default network and executive system contributions to mind wandering. *The Proceedings of the National Academy of Sciences of the United States of America*, *106*, 8719–8724.

Corbetta, M., & Shulman, G. L. (2002). Control of goal-directed and stimulus-driven attention in the brain. *Nature Reviews Neuroscience*, *3*, 201–215.

Deshpande, G., & Hu, X. (2012). Investigating effective brain connectivity from FMRI data: Past findings and current issues with reference to granger causality analysis. *Brain Connectivity*, *2*, 235–245.

Dosenbach, N. U., Fair, D. A., Miezin, F. M., Cohen, A. L., Wenger, K. K., Dosenbach, R. A., ... Petersen, S. E. (2007). Distinct brain networks for adaptive and stable task control in humans. *The Proceedings of the National Academy of Sciences of the United States of America*, *104*, 11073–11078.

Eguiluz, V. M., Chialvo, D. R., Cecchi, G. A., Baliki, M., & Apkarian, A. V. (2005). Scale-free brain functional networks. *Physical Review Letters*, *94*, 18102.

Eldaief, M. C., Halko, M. A., Buckner, R. L., & Pascual-Leone, A. (2011). Transcranial magnetic stimulation modulates the brain's intrinsic activity in a frequency-dependent manner. *The Proceedings of the National Academy of Sciences of the United States of America*, *108*, 21229–21234.

Faes, L., Stramaglia, S., & Marinazzo, D. (2017). On the interpretability and computational reliability of frequency-domain granger causality. *F1000Research*, *6*, 1710.

Finn, E. S., Shen, X., Scheinost, D., Rosenberg, M. D., Huang, J., Chun, M. M., ... Constable, R. T. (2015). Functional connectome fingerprinting: Identifying individuals using patterns of brain connectivity. *Nature Neuroscience*, *18*, 1664–1671.

Fischer, D. B., Boes, A. D., Demertzi, A., Evrard, H. C., Laureys, S., Edlow, B. L., ... Geerling, J. C. (2016). A human brain network derived from coma-causing brainstem lesions. *Neurology*, *87*, 2427–2434.

Fox, M. D., Halko, M. A., Eldaief, M. C., & Pascual-Leone, A. (2012). Measuring and manipulating brain connectivity with resting state functional connectivity magnetic resonance imaging (fcMRI) and transcranial magnetic stimulation (TMS). *NeuroImage*, *62*, 2232–2243.

Fox, M. D., Snyder, A. Z., Vincent, J. L., Corbetta, M., Van Essen, D. C., & Raichle, M. E. (2005). The human brain is intrinsically organized into dynamic, anticorrelated functional networks. *The Proceedings of the National Academy of Sciences of the United States of America*, *102*, 9673–9678.

Friston, K., Moran, R., & Seth, A. K. (2013). Analysing connectivity with granger causality and dynamic causal modelling. *Current Opinion in Neurobiology*, *23*, 172–178.

Gallos, L. K., Makse, H. A., & Sigman, M. (2012). A small world of weak ties provides optimal global integration of self-similar modules in functional brain networks. *The Proceedings of the National Academy of Sciences of the United States of America*, *109*, 2825–2830.

Gratton, C., Lee, T. G., Nomura, E. M., & D'Esposito, M. (2013): The effect of theta-burst TMS on cognitive control networks measured with resting state fMRI. *Frontiers in System Neuroscience 7*, 124. https://www.ncbi.nlm.nih.gov/pmc/articles/PMC3874542/.

Greicius, M. (2008). Resting-state functional connectivity in neuropsychiatric disorders. *Current Opinion in Neurology*, *21*, 424–430.

Halko, M. A., Farzan, F., Eldaief, M. C., Schmahmann, J. D., & Pascual-Leone, A. (2014). Intermittent theta-burst stimulation of the lateral cerebellum increases functional connectivity of the default network. *The Journal of Neuroscience*, *34*, 12049–12056.

Hallett, M. (2007). Transcranial magnetic stimulation: A primer. *Neuron*, *55*, 187–199.

Hearne, L. J., Cocchi, L., Zalesky, A., & Mattingley, J. B. (2017). Reconfiguration of brain network architectures between resting state and complexity-dependent cognitive reasoning. *The Journal of Neuroscience*, *37*, 485–417.

Jbabdi, S., Sotiropoulos, S. N., Haber, S. N., Van Essen, D. C., & Behrens, T. E. (2015). Measuring macroscopic brain connections in vivo. *Nature Neuroscience*, *18*, 1546–1555.

Johnen, V. M., Neubert, F. X., Buch, E. R., Verhagen, L., O'Reilly, J. X., Mars, R. B., & Rushworth, M. F. (2015): Causal manipulation of functional connectivity in a specific neural pathway during behaviour and at rest. *eLife 4*, 941. http://www.ncbi.nlm.nih.gov/pubmed/25664941.

Karabanov, A., Ziemann, U., Hamada, M., George, M. S., Quartarone, A., Classen, J., ... Siebner, H. R. (2015). Consensus paper: Probing homeostatic plasticity of human cortex with noninvasive Transcranial brain stimulation. *Brain Stimulation*, *8*, 442–454.

Koch, G., Fernandez Del, O. M., Cheeran, B., Ruge, D., Schippling, S., Caltagirone, C., & Rothwell, J. C. (2007). Focal stimulation of the posterior parietal cortex increases the excitability of the ipsilateral motor cortex. *The Journal of Neuroscience*, *27*, 6815–6822.

Koch, G., Ponzo, V., Di, L. F., Caltagirone, C., & Veniero, D. (2013). Hebbian and anti-Hebbian spike-timing-dependent plasticity of human cortico-cortical connections. *The Journal of Neuroscience*, *33*, 9725–9733.

Koganemaru, S., Mima, T., Nakatsuka, M., Ueki, Y., Fukuyama, H., & Domen, K. (2009). Human motor associative plasticity induced by paired bihemispheric stimulation. *The Journal of Physiology*, *587*, 4629–4644.

Lustenberger, C., Boyle, M. R., Alagapan, S., Mellin, J. M., Vaughn, B. V., & Fröhlich, F. (2016). Feedback-controlled Transcranial alternating current stimulation reveals a functional role of sleep spindles in motor memory consolidation. *Current Biology*, *26*, 2127–2136.

Madeo, D., Talarico, A., Pascual-Leone, A., Mocenni, C., & Santarnecchi, E. (2017). An evolutionary game theory model of spontaneous brain

functioning. *Scientific Reports*, 7, 15978. https://www.ncbi.nlm.nih.gov/pmc/articles/PMC5700053/

Massimini, M. (2004). The sleep slow oscillation as a traveling wave. *The Journal of Neuroscience*, 24, 6862–6870.

Nee, D. E., & D'Esposito, M. (2016). The hierarchical organization of the lateral prefrontal cortex. *eLife*, 5, e12112.

Nunez, P. L., & Srinivasan, R. (2014). Neocortical dynamics due to axon propagation delays in cortico-cortical fibers: EEG traveling and standing waves with implications for top-down influences on local networks and white matter disease. *Brain Research*, 1542, 138–166.

Pascual-Leone, A., & Walsh, V. (2001). Fast backprojections from the motion to the primary visual area necessary for visual awareness. *Science*, 292, 510–512.

Power, J. D., Cohen, A. L., Nelson, S. M., Wig, G. S., Barnes, K. A., Church, J. A., ... Petersen, S. E. (2011). Functional network organization of the human brain. *Neuron*, 72, 665–678.

Raichle, M. E. (2015). The brain's default mode network. *Annual Review of Neuroscience*, 38, 433–447.

Rizzo, V., Siebner, H. S., Morgante, F., Mastroeni, C., Girlanda, P., & Quartarone, A. (2009). Paired associative stimulation of left and right human motor cortex shapes interhemispheric motor inhibition based on a Hebbian mechanism. *Cerebral Cortex*, 19, 907–915.

Roebroeck, A., Formisano, E., & Goebel, R. (2005). Mapping directed influence over the brain using granger causality and fMRI. *NeuroImage*, 25, 230–242.

Romei, V., Chiappini, E., Hibbard, P. B., & Avenanti, A. (2016). Empowering reentrant projections from V5 to V1 boosts sensitivity to motion. *Current Biology*, 26, 2155–2160.

Rossini, P. M., Burke, D., Chen, R., Cohen, L. G., Daskalakis, Z., Di Iorio, R., ... Ziemann, U. (2015). Noninvasive electrical and magnetic stimulation of the brain, spinal cord, roots and peripheral nerves: Basic principles and procedures for routine clinical and research application. An updated report from an I.F.C.N. Committee. *Clinical Neurophysiology*, 126, 1071–1107.

Santarnecchi, E., Rossi, S., & Rossi, A. (2015): The smarter, the stronger: Intelligence level correlates with brain resilience to systematic insults. *Cortex 64*:293–309.

Sepulcre, J., Liu, H., Talukdar, T., Martincorena, I., Yeo, B. T., & Buckner, R. L. (2010). The organization of local and distant functional connectivity in the human brain. *PLoS Computational Biology*, 6, e1000808.

Seth, A. K., Chorley, P., & Barnett, L. C. (2013). Granger causality analysis of fMRI BOLD signals is invariant to hemodynamic convolution but not downsampling. *NeuroImage*, 65, 540–555.

Shirer, W. R., Ryali, S., Rykhlevskaia, E., Menon, V., & Greicius, M. D. (2012). Decoding subject-driven cognitive states with whole-brain connectivity patterns. *Cerebral Cortex*, 22, 158–165.

Smith, S. M. (2012). The future of FMRI connectivity. *NeuroImage*, 62, 1257–1266.

Sporns, O. (2011). The nonrandom brain: Efficiency, economy, and complex dynamics. *Frontiers in Computational Neuroscience*, 5, 5.

Sporns, O. (2014). Contributions and challenges for network models in cognitive neuroscience. *Nature Neuroscience*, 17, 652–660.

Spreng, R. N., Sepulcre, J., Turner, G. R., Stevens, W. D., & Schacter, D. L. (2013). Intrinsic architecture underlying the relations among the default, dorsal attention, and frontoparietal control networks of the human brain. *Journal of Cognitive Neuroscience*, 25, 74–86.

Spreng, R. N., Stevens, W. D., Chamberlain, J. P., Gilmore, A. W., & Schacter, D. L. (2010). Default network activity, coupled with the frontoparietal control network, supports goal-directed cognition. *NeuroImage*, 53, 303–317.

Spreng, R. N., Stevens, W. D., Viviano, J. D., & Schacter, D. L. (2016). Attenuated anticorrelation between the default and dorsal attention networks with aging: Evidence from task and rest. *Neurobiology of Aging*, 45, 149–160.

Stefan, K., Kunesch, E., Benecke, R., Cohen, L. G., & Classen, J. (2002). Mechanisms of enhancement of human motor cortex excitability induced by interventional paired associative stimulation. *The Journal of Physiology*, 543, 699–708.

Stokes, P. A., & Purdon, P. L. (2017). A study of problems encountered in granger causality analysis from a neuroscience perspective. *Proceedings of the National Academy of Sciences of the United States of America*, 114, E7063–E7072.

Tavor, I., Parker, J. O., Mars, R. B., Smith, S. M., Behrens, T. E., & Jbabdi, S. (2016). Task-free MRI predicts individual differences in brain activity during task performance. *Science*, 352, 216–220.

Thiebaut de Schotten, M., Urbanski, M., Batrancourt, B., Levy, R., Dubois, B., Cerliani, L., & Volle, E. (2017). Rostro-caudal architecture of the frontal lobes in humans. *Cerebral Cortex New York 1991*, 27, 4033–4047.

Tomasi, D., Ernst, T., Caparelli, E. C., & Chang, L. (2006). Common deactivation patterns during working memory and visual attention tasks: An intra-subject fMRI study at 4 tesla. *Human Brain Mapping*, 27, 694–705.

Tseng, P., Hsu, T. Y., Chang, C. F., Tzeng, O. J., Hung, D. L., Muggleton, N. G., ... Juan, C. H. (2012). Unleashing potential: Transcranial direct current stimulation over the right posterior parietal cortex improves change detection in low-performing individuals. *Journal of Neuroscience*, 32, 10554–10561.

Turrigiano, G. G. (2008). The self-tuning neuron: Synaptic scaling of excitatory synapses. *Cell*, 135, 422–435.

Uddin, L. Q. (2014). Salience processing and insular cortical function and dysfunction. *Nature Reviews. Neuroscience*, 16, 55–61.

Veniero, D., Ponzo, V., & Koch, G. (2013). Paired associative stimulation enforces the communication between interconnected areas. *The Journal of Neuroscience*, 33, 13773–13783.

Vicente, R., Wibral, M., Lindner, M., & Pipa, G. (2011). Transfer entropy—A model-free measure of effective connectivity for the neurosciences. *Journal of Computational Neuroscience*, 30, 45–67.

Wang, J. X., Rogers, L. M., Gross, E. Z., Ryals, A. J., Dokucu, M. E., Brandstatt, K. L., ... Voss, J. L. (2014). Targeted enhancement of cortical-hippocampal brain networks and associative memory. *Science*, 345, 1054–1057.

Wibral, M., Vicente, R., & Lindner, M. (2014). Transfer entropy in neuroscience. In *Directed information measures in neuroscience* (pp. 3–36). Berlin, Heidelberg: Springer. https://link.springer.com/chapter/10.1007/978-3-642-54474-3_1

Worsley, K. J., Marrett, S., Neelin, P., Vandal, A. C., Friston, K. J., & Evans, A. C. (1996). A unified statistical approach for determining significant signals in images of cerebral activation. *Human Brain Mapping*, 4, 58–73.

Yeo, B. T., Krienen, F. M., Sepulcre, J., Sabuncu, M. R., Lashkari, D., Hollinshead, M., ... Buckner, R. L. (2011). The organization of the human cerebral cortex estimated by intrinsic functional connectivity. *Journal of Neurophysiology*, 106, 1125–1165.

Zheng, P., Dimitrakakis, C., & Triesch, J. (2013). Network self-organization explains the statistics and dynamics of synaptic connection strengths in cortex. *PLoS Computational Biology*, 9, e1002848.

Zhou, J., Greicius, M. D., Gennatas, E. D., Growdon, M. E., Jang, J. Y., Rabinovici, G. D., ... Seeley, W. W. (2010). Divergent network connectivity changes in behavioural variant frontotemporal dementia and Alzheimer's disease. *Brain*, 133, 1352–1367.

Zhou, Y., Friston, K. J., Zeidman, P., Chen, J., Li, S., & Razi, A. (2018). The hierarchical Organization of the Default, dorsal attention and salience networks in adolescents and young adults. *Cerebral Cortex*, 28, 726–737.

SUPPORTING INFORMATION

Additional supporting information may be found online in the Supporting Information section at the end of the article.